The Journal of Chemical Physics

Understanding the lithiation limits of high-capacity organic battery anodes by atomic charge derivative analysis

Cite as: J. Chem. Phys. **157**, 181101 (2022); https://doi.org/10.1063/5.0119904
Submitted: 10 August 2022 • Accepted: 18 October 2022 • Accepted Manuscript Online: 18 October 2022 • Published Online: 08 November 2022

Rodrigo P. Carvalho, Cleber F. N. Marchiori, Daniel Brandell, et al.

The Journal of Chemical Physics COMMUNICATION scitation.org/journal/jcp

Understanding the lithiation limits of high-capacity organic battery anodes by atomic charge derivative analysis

Cite as: J. Chem. Phys. 157, 181101 (2022); doi: 10.1063/5.0119904
Submitted: 10 August 2022 • Accepted: 18 October 2022 •
Published Online: 8 November 2022

Rodrigo P. Carvalho,[1,2,a)] Cleber F. N. Marchiori,[3] Daniel Brandell,[2] and C. Moyses Araujo[1,3,a)]

AFFILIATIONS

[1] Materials Theory Division, Department of Physics and Astronomy, Uppsala University, Box 516, 75120 Uppsala, Sweden
[2] Department of Chemistry, Ångström Laboratory, Uppsala University, Box 538, 75121 Uppsala, Sweden
[3] Department of Engineering and Physics, Karlstad University, 65188 Karlstad, Sweden

Note: This paper is part of the JCP Special Topic on Chemical Physics of Electrochemical Energy Materials.
[a)]**Authors to whom correspondence should be addressed:** rodrigo.carvalho@physics.uu.se and Moyses.Araujo@kau.se

ABSTRACT

The *superlithiation* of organic anodes is a promising approach for developing the next generation of sustainable Li-ion batteries with high capacity. However, the lack of fundamental understanding hinders its faster development. Here, a systematic study of the lithiation processes in a set of dicarboxylate-based materials is carried out within the density functional theory formalism. It is demonstrated that a combined analysis of the Li insertion reaction thermodynamics and the conjugated-moiety charge derivative enables establishing the experimentally observed maximum storage, thus allowing an assessment of the structure–function relationships also.

INTRODUCTION

The rapid implementation of Li-ion batteries has highlighted some of the problems of this technology, which has sparked interest in organic-based electrode materials.[1–3] They present a feasible alternative to conventional inorganic-based compounds in key aspects related to environmental issues, such as mining impacts and recyclability.[4–6] In recent years, several organic compounds have been reported as functional active electrode materials for Li-,[7–11] Na-,[12–14] and K-ion[15–18] batteries for a range of different chemistries.[19–23] Some of these materials can offer long cyclability,[24–26] high specific energy,[27,28] and fast kinetics.[29,30] In particular, the dicarboxylate-based compounds display promising properties in terms of comparatively high capacity, decent kinetics, and also being abundant in nature, thereby constituting a platform that can utilize biological resorces.[31] These compounds present a rich variety of reaction mechanisms, which are intrinsically dependent on their organic-chemistry functionalities. In this context, the reversible reduction of the carbonyl (R–C=O) oxygen double bond during the coupled electron–ion de/insertion process has been utilized extensively. For high potential electrodes, the inserted electron tends to be localized over the redox active centers, while for low potential electrodes it tends to be delocalized over the moiety, with the molecular unit functioning as an electronic reservoir in both cases.[32,33] For some compounds, however, the amount of charge this organic reservoir accepts can surpass what is expected, thereby directly affecting the maximum number of ions to be inserted. Such abnormal capacity to store Li-ions has been reported for a number of dicarboxylate-based compounds.[34–37] Dilithium benzene-dipropiolate (Li_2BDP),[35] for example, has been shown to accommodate 11.5 Li-ions per molecular unit ($Li_{13.5}BDP$). This represents an excess of 5.5 Li-ions per molecular unit over the expected capacity estimated by considering the possible reduction sites. On the other hand, the structurally fairly similar dilithium benzene diacrylate (Li_2BDA)[33,38] does not exhibit this behavior, allowing insertion of only two Li-ions (Li_4BDA), i.e., the expected reduction of the two carbonyl groups.

This "superlithiation" phenomenon is still poorly understood, and a systematic way to describe the electric storage limits of these organic materials is yet to be realized. Furthermore,

understanding the fundamental aspects of this storage mechanism constitutes a necessary step to design novel battery electrodes that could offer superior energy storage capacity. Herein, we report an investigative analysis at a molecular level to probe the charge storage limits of a set of dicarboxylate-based organic electroactive materials: dilithium acetylene-dicarboxylate (Li_2ADC), dilithium tolane-dicarboxylate (Li_2TODC),[39] dilithium thiophene-dicarboxylate (Li_2TDC),[34,40] dilithium terephthalate (Li_2TP),[31,32] and the already mentioned Li_2BDA and Li_2BDP. The Lewis structures of these compounds are shown in Fig. 1(a). Together, they span a space of carbonyl-based materials with different functionalities, where some show the superlithiation behavior and some not due to still unknown reasons, while all are of low M_w enough to provide a robust benchmarking. The computational approach starts by performing a microcanonical (NVE) Born–Oppenheimer molecular dynamics simulation at a reasonably high temperature (400 K) for several lithiation stages. This *ab initio* molecular dynamics (AIMD) simulations-based approach is carried out following the density functional theory (DFT) framework as implemented in the Vienna Ab initio Simulation Package (VASP) code.[41–43] The elevated temperature allows the configurational space of these molecules to be explored during the dynamics, which helps to understand the

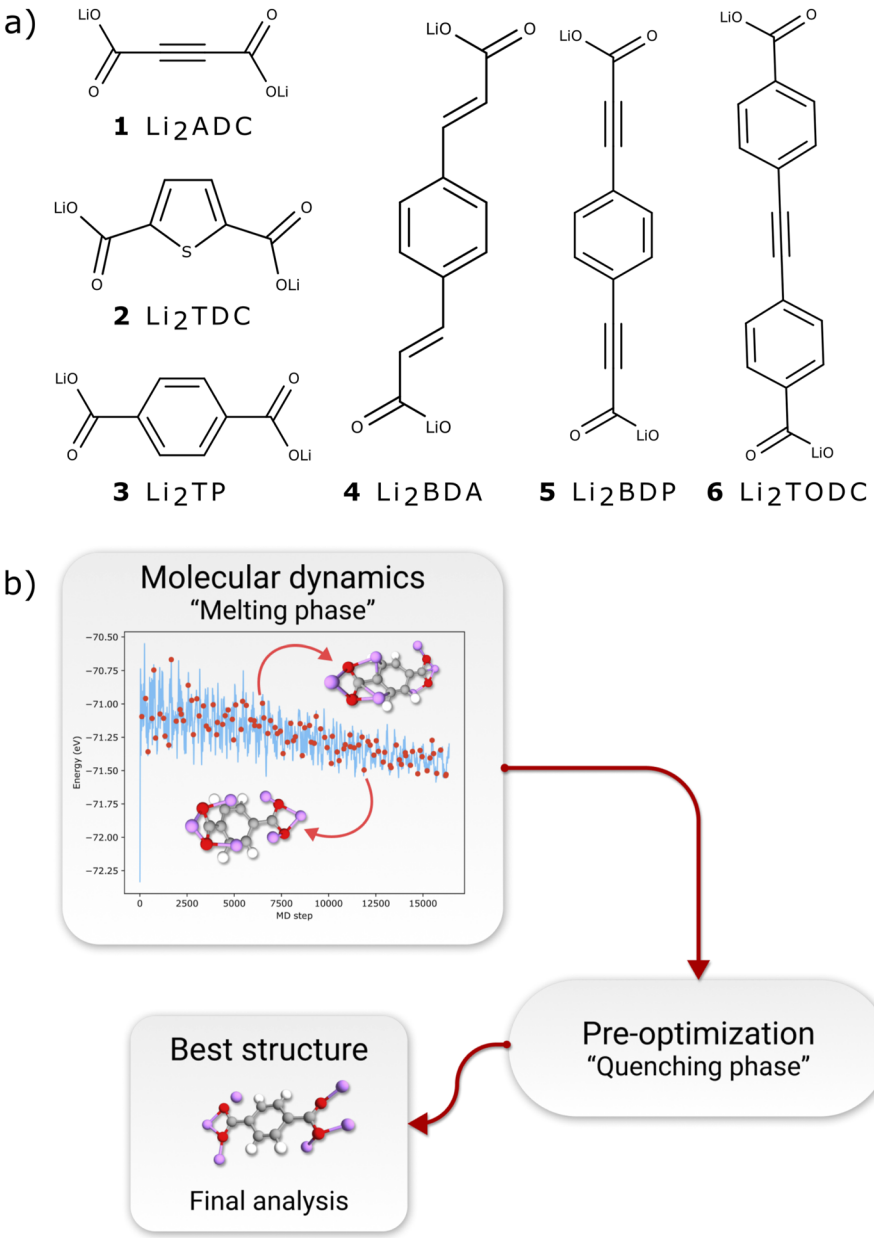

FIG. 1. (a) 2D representations of all the investigated compounds. (b) Workflow summarizing the melting–quenching framework employed in this work. The following color scheme applies for the atoms: pink for lithium, white for hydrogen, gray for carbon, and red for oxygen.

Li-ion positioning relative to the moiety. Although this methodology does not reflect the complete electrode environment, it mimics well the intrinsic molecular-level changes, which are the most essential for the reactions. In contrast to most conventional Li-ion battery electrodes, these materials form molecular crystals, which largely preserve the properties of the molecular building blocks. Furthermore, alternatively assessing all the lithiated phases of a given compound is unrealistic due to computational limitations, at least if done in a sophisticated manner. For instance, if an accurate prediction technique such as the evolutionary algorithm[33] is be considered, a substantial computational effort is required to predict all phases of a compound like Li_2BDP that has a final lithiation state of $Li_{13.5}$BDP. This motivates the choice of the applied methodology.

In sequence, the AIMD simulation was split into 100 equal intervals and one random snapshot was chosen from each of them, resulting in 100 snapshots from equally spaced time intervals. Then, geometry optimizations were performed on all these structures following the VASP DFT framework, selecting in sequence the one with the lowest ground-state electronic energy. This final structure then served as a starting point for further investigations, such as the thermodynamics of the lithiation reaction. This entire process, also known as a "melting-quenching" approach,[44–46] is summarized in Fig. 1(b) and one of its major features is to find the most stable configuration within the proposed limits. Nonetheless, a final geometry optimization within the DFT framework was performed for all selected structures following the implementation present in the Gaussian 16 software package.[47] More details are provided in the supplementary material. From this step, a Natural Population Analysis[48] was also performed to evaluate atomic charges. Furthermore, several lithiation stages were evaluated for all investigated compounds together with their Li-ion insertion thermodynamics and formation energies to uncover possible reaction pathways. These quantities were obtained by following the Nernst equation and the formation energy of alloys, i.e., Eqs. (S2) and (S3), respectively.

Figure 2 shows the Li-ion insertion voltages for different reaction pathways, following the corresponding reaction thermodynamics and formation energies of the involved phases. These pathways are expressed by a sequence of numbers (shown in Fig. 2) representing the total amount of Li-ions in the compound, always starting from the delithiated phase. In short, a sequence of "2, 3, 4, 6" means that 1 Li^+ is first inserted in this material (Li_2 -> Li_3), followed by another one (Li_3 -> Li_4) and finally a two-step reaction of 2 Li^+ (Li_4 -> Li_6). To evaluate the actual phases participating in these reactions, thermodynamic analysis suggests that the equilibrium potential $V(n)$ with respect to Li/Li^+ should decrease or stay constant for each lithiation step n. Equivalently,

$$\frac{\partial V(n)}{\partial n} \leq 0, \tag{1}$$

which means that the potential should always decrease upon Li^+ insertion. Therefore, phases that violate this rule or have unfavorable formation energies [Eq. (S3)] should not be observed. In such cases, the system disproportionates into an equilibrium mixture of the previous and the next phases (if the overall thermodynamics of such reaction is favored), which may occur through a two-step process in the electrode. Figure 2(a) shows the Li_2ADC case, following two allowed reaction pathways. This molecule is expected to accommodate 4 Li^+ (Li_6ADC) upon reduction of the carbonyl groups and the carbon–carbon triple bond (C≡C). However, our analysis shows that it can be further lithiated up to the Li_9ADC phase, i.e., an excess of three Li-ions. Considering the small molecular weight of this compound, this represents an impressive lithiation capacity. Similarly, Fig. 2(b) presents the Li_2TODC being reduced to Li_4TODC, in accordance with the results reported by Tarascon and colleagues.[39] Nonetheless, our thermodynamic analysis suggests that the Li_5TODC and Li_6TODC phases are also thermodynamically favorable. Li_2TDC, in Fig. 2(c), has been shown to accommodate an "abnormal" capacity in the work of Lee *et al.*,[34] reaching the $Li_{7.8}$TDC phase instead of the expected Li_4TDC phase based on the reduction of carbonyls. Likewise, our analysis suggests that this material can be lithiated up to Li_7TDC or Li_8TDC phases. However, the molecular ring is fragmented during the Li_8TDC AIMD simulation, leading to a degradation process. This effect is also reported experimentally, with an increasing amorphization being observed during the initial cycles. In the same work from Lee *et al.*,[34] a similar "abnormal" capacity is shown for Li_2TP, with the material undergoing two extra lithiation steps (Li_6TP). Figure 2(d) shows that this material can in fact be further reduced to Li_8TP, i.e., an additional two-step reaction could occur. For Li_2BDA, in Fig. 2(e), two different reaction pathways are possible. The first shows that the lithiation could go up to the Li_{10}BDA phase, while the other set shows a maximum at Li_5BDA. However, this material is reported[38] to accommodate only two inserted Li-ions, i.e., Li_4BDA would be its final stage. This possible overestimation of the storage capacity illustrates the limitations of the current approach, which is purely based on the reaction thermodynamics. Finally, Fig. 2(f) shows the compound Li_2BDP. As previously stated, this compound was reported to achieve an impressive lithiation capacity of 11.5 inserted Li-ions, stabilizing into the $Li_{13.5}$BDP phase.[35] Our analysis suggests that this material could reach either the Li_{12}BDP or Li_{14}BDP phase, depending on the reaction pathway. Given the experimental result ($Li_{13.5}$BDP), it is possible that both phases with 12 and 14 Li-ions are being stabilized during the battery operation, hence the displayed "average" equilibrium phase with 13.5 Li-ions.

Only analyzing the insertion voltages is actually insufficient to evaluate the maximum storage capacity of these materials. The dilithium terephthalate case, for example, shows that this material could be reduced to the Li_8TP phase; however, only the Li_6TP phase has been experimentally observed.[34] To address this issue, we introduce a charge variation analysis of the organic moiety. The organic counterpart (excluding Li-ions) here functions as a charge reservoir, accommodating the inserted electron at each lithiation step. Therefore, following the changes in the charge state of the moiety probes their capacity limit. In particular, the charge variation for each lithiation step n should be negative when the moiety accepts the inserted electron and positive otherwise. This can also be formulated according to the following equation:

$$\frac{\partial Q(n)}{\partial n} < 0, \tag{2}$$

where Q represents the total charge of the moiety (in units of e), excluding Li-ions. Therefore, this derivative will be positive at the limit where the material would fail in accommodating extra

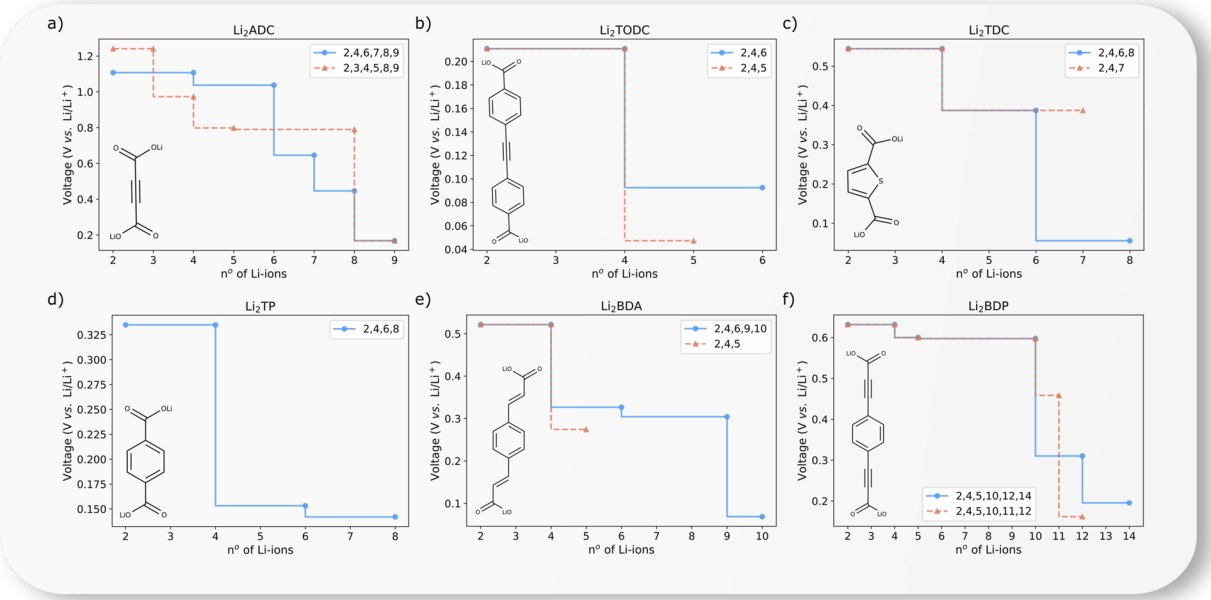

FIG. 2. Insertion open-circuit voltages of the different reaction pathways for the (a) Li_2ADC, (b) Li_2TODC, (c) Li_2TDC, (d) Li_2TP, (e) Li_2BDA, and (f) Li_2BDP compounds.

electrons. At the molecule level, the moiety reduction starts to become less favorable than the reduction of Li-ions, which would lead to the electron being transferred to the Li^+ and, thus, the formation of metallic Li. This process may also be seen as the oxidation potential of the succeeding phase becoming more positive than the Li^+ reduction potential. In this context, Fig. 3(a) shows the average charge per atom (excluding Li) as a function of the number of Li-ions, while the zero-charge level refers to the delithiated compound. These averages were calculated according to Eq. S(4). Phases not following Eq. (1) or showing an unfavorable formation energy were excluded from this analysis. The slope at different reaction steps in these plots corresponds to Eq. (2) and is connected to the charge storage capacity of the material. For example, a downward slope represents a negative derivate—i.e., the moiety can accommodate more charge—while an upward change represents a positive value in Eq. (2). For all the investigated compounds, the charge varies according to the expected behavior. For example, BDP shows a constant decrease in charge over the continuous reaction steps, while TP displays an ascending slope after the Li_6TP phase, signaling that this would be its limit. The TDC, on the other hand, seems to saturate at the Li_6 phase, but a steep descent slope appears at the Li_8 phase. This is a result of the degradation process shown during the AIMD simulation, with the ring being fragmented. Furthermore, the charge derivatives are shown in Figs. 3(b)–3(g) for the possible reaction pathways discussed before. These derivatives are obtained from the total charge of the moiety in each reduction step, excluding Li. Figure 3(b) shows the Li_2ADC case, with a positive derivative appearing for Li_{10}ADC. Correspondingly, for this phase, the moiety repels one Li-ion during the AIMD simulation. Figure S1 shows the Li coordination number evolution during the AIMD simulation for each reduction step, with the appearance of a coordination number of 0 for the Li_{10} phase, i.e., the Li is repelled by the moiety. For Li_2TODC, Fig. 3(c) shows both reaction pathways with negative derivative, but the Li_6TODC phase display a relatively small value. This indicates that the moiety is likely to fail to accommodate the inserted electron. Furthermore, the equilibrium potential (Fig. 2) to reach Li_5TODC is also rather small (near 0.05 V vs Li/Li^+). These combined observations suggest that both phases are not easily accessible during lithiation; hence, the insertion of 2 Li^+ (Li_4TODC) should be the limiting capacity for this compound. Figure 3(d), in turn, shows that the Li_2TDC compound has a zero derivative for the Li_7TDC phase, i.e., the moiety does not favor this reduction reaction. In addition, Fig. S2 also shows a Li coordination number of 0 appearing for this phase. However, the derivate shows a significant drop for Li_8TDC. This happens following the reduction of the carbon–sulfur bonds in the thiophene ring and results in a degradation of the molecule. Therefore, the experimentally observed $Li_{7.8}$TDC phase may be achieved through a degradation of the thiophene rings, which corresponds well with the progressive amorphization reported for this compound.[34] For Li_2TP in Fig. 3(e), the charge derivative for the Li_8TP phase is close to zero, and therefore the TP moiety starts to fail in accommodating new electrons. This result is in conformity with the experimental finding of Li_6TP being the final stabilized phase. Furthermore, the moiety starts to repel a Li-ion in the Li_7TP phase, and a Li coordination number of 0 is shown in Fig. S3 for this and the Li_8TP phases. Figure 3(f) shows the benzene diacrylate case, with a positive derivative appearing for the Li_5BDA phase. As can be seen, our results suggest that this moiety could be further reduced as far as to the Li_9BDA phase, if another reaction path is considered. However,

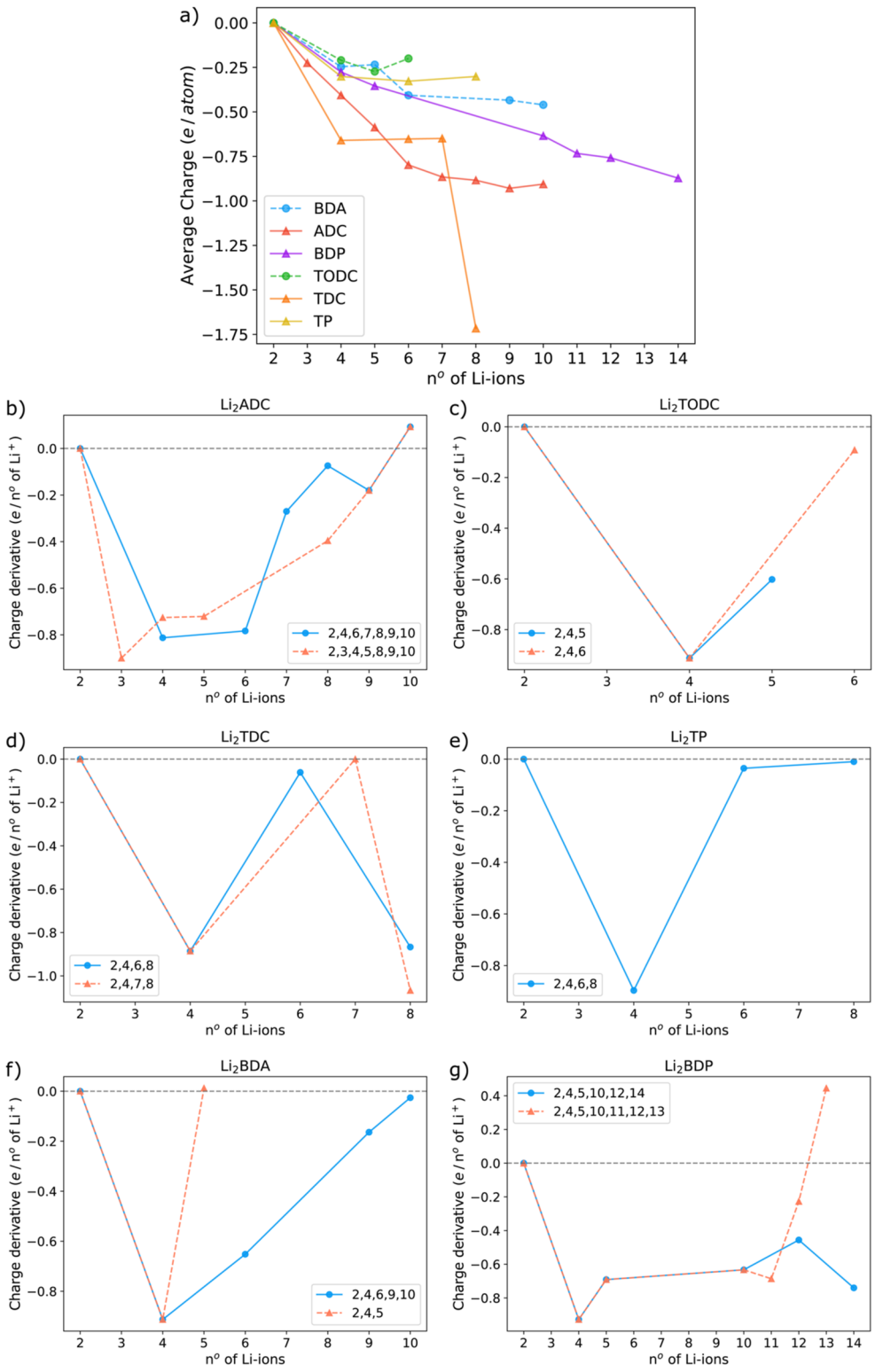

FIG. 3. (a) Average charge per atom (excluding Li) as a function of the number of Li-ions and referred to the pristine phase. The charge derivatives for the (b) Li_2ADC, (c) Li_2TODC, (d) Li_2TDC, (e) Li_2TP, (f) Li_2BDA, and (g) Li_2BDP compounds.

this compound has experimentally been reported to be lithiated only to the Li_4BDA phase. The nonobservance of further reduction steps, contrary to our analysis, may be connected to the existence of higher activation barriers for the $Li_4BDA + 2(Li^+ + e^-) \rightarrow Li_6BDA$ reaction. Otherwise, these further lithiation states not being experimentally observed may be a feature of the experimental measurements themselves. In the reported findings,[38] the Li_2BDA compound was cycled in the potential ranges of 0.9–3.0 V vs Li/Li^+. However, the "extra" Li-ions are predicted to be inserted at much lower potentials than 0.9 V.

Nevertheless, the results in Fig. 3 highlight the shortcomings of the insertion voltages analysis depicted in Fig. 2 and better illustrate the contrasts of the different reaction pathways. Finally, Li_2BDP in Fig. 3(g) shows a positive derivative first for the $Li_{12} \rightarrow Li_{13}$ step. Therefore, the moiety could be reduced up to the $Li_{14}BDP$ phase, as observed experimentally ($Li_{13.5}BDP$).[35] Moreover, the final $Li_{13.5}BDP$ phase is once again justified as an intermediate of both $Li_{12}BDP$ and $Li_{14}BDP$ phases.

CONCLUSIONS

In summary, the joint analysis of Li-ion insertion reaction thermodynamics for these compounds and the corresponding charge derivatives is fundamental for understanding the lithiation limit in organic battery electrodes. It is seen that these charge derivatives are directly connected with the organic moiety's ability to be consecutively reduced, i.e., its ability to accommodate new inserted electrons during lithiation. Thereby, it becomes an important fingerprint to understand the energy storage mechanism in these materials, complementing the conventional reaction thermodynamic analysis. Moreover, our results are in good alignment with the experimental reports for all the electrodes investigated. It is also vital that this framework can be employed to uncover the possible reaction pathways during lithiation, e.g., plausible one- or two-phase reactions. Finally, our findings provide a thermodynamic explanation to the "superlithiation" phenomenon[36,37,49,50] reported in the battery literature and unveil the lithiation limits of organic electroactive materials.

SUPPLEMENTARY MATERIAL

The supplementary material contains a detailed description of the methodology and theoretical framework, additional figures [Figs. S1–S3], equations [Eqs. (S1)–(S4)] and the final molecular geometries for all the different compounds and phases.

ACKNOWLEDGMENTS

The authors acknowledge support from the Swedish Research Council (Grant Nos. 2018-04506 and 2020-05223), the Swedish Energy Agency (Grant No. 45420-1), and STandUP for Energy. The computational infrastructure was provided by the Swedish National Infrastructure for Computing (SNIC) at the National Supercomputer Centre (NSC) at Linköping University.

AUTHOR DECLARATIONS

Conflict of Interest

The authors have no conflicts to disclose.

Author Contributions

Rodrigo P. Carvalho: Conceptualization (equal); Data curation (lead); Formal analysis (equal); Investigation (lead); Methodology (equal); Software (lead); Validation (equal); Visualization (lead); Writing – original draft (lead); Writing – review & editing (equal). **Cleber F. N. Marchiori**: Conceptualization (supporting); Data curation (supporting); Formal analysis (supporting); Investigation (supporting); Writing – review & editing (equal). **Daniel Brandell**: Conceptualization (equal); Funding acquisition (equal); Methodology (equal); Project administration (equal); Resources (equal); Supervision (equal); Writing – review & editing (equal). **C. Moyses Araujo**: Conceptualization (equal); Data curation (supporting); Formal analysis (supporting); Funding acquisition (equal); Investigation (equal); Methodology (equal); Project administration (equal); Resources (equal); Supervision (equal); Validation (equal); Writing – review & editing (equal).

DATA AVAILABILITY

The data that support the findings of this study are available within the article and its supplementary material.

REFERENCES

[1] D. Larcher and J.-M. Tarascon, Nat. Chem. **7**, 19–29 (2015).
[2] C. P. Grey and J. M. Tarascon, Nat. Mater. **16**, 45–56 (2017).
[3] B. Esser, F. Dolhem, M. Becuwe, P. Poizot, A. Vlad, and D. Brandell, J. Power Sources **482**, 228814 (2021).
[4] H. Chen, M. Armand, G. Demailly, F. Dolhem, P. Poizot, and J.-M. Tarascon, ChemSusChem **1**, 348–355 (2008).
[5] S. Renault, D. Brandell, and K. Edström, ChemSusChem **7**, 2859–2867 (2014).
[6] Z. Song and H. Zhou, Energy Environ. Sci. **6**, 2280–2301 (2013).
[7] L. Fédèle, O. Ouari, F. Sauvage, A. Thiam, and M. Becuwe, ChemSusChem **13**, 2321–2327 (2020).
[8] Y. Liang, Z. Tao, and J. Chen, Adv. Energy Mater. **2**, 742–769 (2012).
[9] B. Haeupler, A. Wild, and U. S. Schubert, Adv. Energy Mater. **5**, 1402034 (2015).
[10] R. P. Fornari and P. de Silva, Wiley Interdiscip Rev Comput. Mol. Sci. **11**, e1495 (2021).
[11] T. B. Schon, B. T. McAllister, P.-F. Li, and D. S. Seferos, Chem. Soc. Rev. **45**, 6345–6404 (2016).
[12] M. Lee, J. Hong, J. Lopez, Y. Sun, D. Feng, K. Lim, W. C. Chueh, M. F. Toney, Y. Cui, and Z. Bao, Nat. Energy **2**, 861–868 (2017).
[13] Y. Xu, M. Zhou, and Y. Lei, Mater. Today **21**, 60–78 (2018).
[14] X. Yin, S. Sarkar, S. Shi, Q. A. Huang, H. Zhao, L. Yan, Y. Zhao, and J. Zhang, Adv. Funct. Mater. **30**, 1908445 (2020).
[15] B. Tian, J. Zheng, C. Zhao, C. Liu, C. Su, W. Tang, X. Li, and G.-H. Ning, J. Mater. Chem. A **7**, 9997–10003 (2019).
[16] A. Slesarenko, I. K. Yakuschenko, V. Ramezankhani, V. Sivasankaran, O. Romanyuk, A. v. Mumyatov, I. Zhidkov, S. Tsarev, E. Z. Kurmaev, A. F. Shestakov, O. v. Yarmolenko, K. J. Stevenson, and P. A. Troshin, J. Power Sources **435**, 226724 (2019).
[17] S. Xu, Y. Chen, and C. Wang, J. Mater. Chem. A **8**, 15547–15574 (2020).
[18] W. Zhang, W. Huang, and Q. Zhang, Chem. - Eur. J. **27**, 6131–6144 (2021).
[19] S. Lee, J. E. Kwon, J. Hong, S. Y. Park, and K. Kang, J. Mater. Chem. A **7**, 11438–11443 (2019).
[20] T. Yokoji, H. Matsubara, and M. Satoh, J. Mater. Chem. A **2**, 19347–19354 (2014).
[21] X. Fan, F. Wang, X. Ji, R. Wang, T. Gao, S. Hou, J. Chen, T. Deng, X. Li, L. Chen, C. Luo, L. Wang, and C. Wang, Angew. Chem., Int. Ed. Engl. **57**, 7146–7150 (2018).
[22] S. Lee, J. Hong, K. Kang, S. Lee, K. Kang, and J. Hong, Adv. Energy Mater. **10**, 2001445 (2020).

[23]P. Xu, D. H. S. Tan, and Z. Chen, Trends Chem. **3**, 620–630 (2021).
[24]P. Acker, L. Rzesny, C. F. N. Marchiori, C. M. Araujo, and B. Esser, Adv. Funct. Mater. **29**, 1906436 (2019).
[25]A. Iordache, D. Bresser, S. Solan, M. Retegan, M. Bardet, J. Skrzypski, L. Picard, L. Dubois, and T. Gutel, Advanced Sustainable Systems **1**, 1600032 (2017).
[26]S. Bai, B. Kim, C. Kim, O. Tamwattana, H. Park, J. Kim, D. Lee, and K. Kang, Nat. Nanotechnol. **16**, 77–84 (2020).
[27]A. Jouhara, N. Dupré, A.-C. Gaillot, D. Guyomard, F. Dolhem, and P. Poizot, Nat. Commun. **9**, 4401 (2018).
[28]A. Shimizu, Y. Tsujii, H. Kuramoto, T. Nokami, Y. Inatomi, N. Hojo, and J.-i. Yoshida, Energy Technol. **2**, 155–158 (2014).
[29]S. Muench, A. Wild, C. Friebe, B. Häupler, T. Janoschka, and U. S. Schubert, Chem. Rev. **116**, 9438–9484 (2016).
[30]K. Oyaizu and H. Nishide, Adv. Mater. **21**, 2339–2344 (2009).
[31]M. Armand, S. Grugeon, H. Vezin, S. Laruelle, P. Ribière, P. Poizot, and J.-M. Tarascon, Nat. Mater. **8**, 120–125 (2009).
[32]R. P. Carvalho, C. F. N. Marchiori, D. Brandell, and C. M. Araujo, ChemSusChem **13**, 2402–2409 (2020).
[33]R. P. Carvalho, C. F. N. Marchiori, V.-A. Oltean, S. Renault, T. Willhammar, C. Pay Gómez, C. M. Araujo, and D. Brandell, Mater. Adv. **2**, 1024–1034 (2021).
[34]H. H. Lee, Y. Park, K.-H. Shin, K. T. Lee, and S. Y. Hong, ACS Appl. Mater. Interfaces **6**, 19118–19126 (2014).
[35]S. Renault, V. A. Oltean, C. M. Araujo, A. Grigoriev, K. Edström, and D. Brandell, Chem. Mater. **28**, 1920–1926 (2016).
[36]B. T. McAllister, E. Grignon, T. B. Schon, S. Y. An, C.-H. Yim, Y. Abu-Lebdeh, and D. S. Seferos, ACS Appl. Energy Mater. **4**, 6659–6666 (2021).
[37]X. Dong, B. Ding, H. Guo, H. Dou, and X. Zhang, ACS Appl. Mater. Interfaces **10**, 38101–38108 (2018).
[38]V. A. Mihali, S. Renault, L. Nyholm, and D. Brandell, RSC Adv. **4**, 38004–38011 (2014).
[39]W. Walker, S. Grugeon, H. Vezin, S. Laruelle, M. Armand, F. Wudl, and J.-M. Tarascon, J. Mater. Chem. **21**, 1615–1620 (2011).
[40]C. F. N. Marchiori, D. Brandell, and C. M. Araujo, J. Phys. Chem. C **123**, 4691–4700 (2019).
[41]G. Kresse and D. Joubert, Phys. Rev. B **59**, 1758–1775 (1999).
[42]G. Kresse and J. Hafner, Phys. Rev. B **47**, 558–561 (1993).
[43]G. Kresse and J. Furthmüller, Phys. Rev. B **54**, 11169–11186 (1996).
[44]T. Shimizu and T. Yamamoto, J. Chem. Phys. **113**, 3351 (2000).
[45]W. L. Scopel, A. J. R. da Silva, and A. Fazzio, Phys Rev. B **77**, 172101 (2008).
[46]K. Tanwar, X. Tan, M. M. Rahman, S. Mateti, P. Cizek, P. Koley, C. Hou, S. C. Smith, and Y. Chen, J. Power Sources **511**, 230445 (2021).
[47]M. J. Frisch, G. W. Trucks, H. E. Schlegel, G. E. Scuseria, M. A. Robb, J. R. Cheeseman, G. Scalmani, V. Barone, G. A. Petersson, O. Farkas, J. B. Foresman, and J. D. Fox, GAUSSIAN, Inc., Wallingford CT, 2016.
[48]A. E. Reed, R. B. Weinstock, and F. Weinhold, J. Chem. Phys. **83**, 735 (1998).
[49]F. Jiang, Y. Wang, T. Qiu, Y. Zhang, W. Zhu, C. Yang, J. Huang, Z. Fang, and G. Dai, ACS Appl. Mater. Interfaces **13**, 48818–48827 (2021).
[50]H. Yang, S. Liu, L. Cao, S. Jiang, and H. Hou, J. Mater. Chem. A **6**, 21216–21224 (2018).